SLAC-PUB-6437
January 1994
T/E

RADIATIVE B DECAYS*

J.L. HEWETT
Stanford Linear Accelerator Center
Stanford University, Stanford, CA 94309

ABSTRACT

We summarize the constraints placed on physics beyond the Standard Model from the recent CLEO observation of the exclusive decay $B \to K^*\gamma$ and bound on the inclusive mode $b \to s\gamma$.

The Standard Model (SM) of electroweak interactions is in complete agreement with present experimental data[1]. Nonetheless, it is believed to leave many questions unanswered, and this belief has resulted in numerous attempts to discover a more fundamental underlying theory. The search for new physics is conducted via a three-prong attack: (i) direct production of new particles at high energy colliders, (ii) deviations from SM predictions in precision measurements, and (iii) indirect observation of new physics in rare or forbidden processes. This talk will focus on the latter option, and in particular will examine the weak radiative B decay $b \to s\gamma$. CLEO has recently[2] observed the exclusive decay $B \to K^*\gamma$ with a branching fraction of $B(B \to K^*\gamma) = (4.5 \pm 1.5 \pm 0.9) \times 10^{-5}$ and has also placed an upper limit on the underlying quark-level process of $B(b \to s\gamma) < 5.4 \times 10^{-4}$ at the 95% C.L. Using a conservative value of the ratio of exclusive to inclusive decay rates based on lattice calculations[3], the CLEO observation of the exclusive process also implies the lower bound $B(b \to s\gamma) > 0.65 \times 10^{-4}$ at 95% C.L. On the theoretical side, the reliability of the calculation of the quark-level process $b \to s\gamma$ has been improved with the inclusion of the next-to-leading logarithmic QCD corrections[4] to the effective Hamiltonian. These new experimental and theoretical results have inspired a large volume of recent literature[5], which can be summarized by the following list:

- "Top Ten" Models Constrained by $b \to s\gamma$

1. Standard Model
2. Anomalous Top-Quark Couplings
3. Anomalous Trilinear Gauge Couplings
4. Fourth Generation
5. Two-Higgs-Doublet Models
6. Supersymmetry
7. Three-Higgs-Doublet Model
8. Extended Technicolor
9. Leptoquarks
10. Left-Right Symmetric Models

Clearly, I can only discuss a couple of these models here, a more complete review can be found in Ref. [5].

In the SM, the quark-level transition $b \to s\gamma$ is mediated by W-boson and t-quark exchange in an electromagnetic penguin diagram. To obtain the branching fraction, the inclusive rate is scaled to that of the semi-leptonic decay $b \to X\ell\nu$. This procedure removes uncertainties in the calculation due to an overall factor of m_b^5 which appears in both expressions, and reduces the ambiguities involved with the imprecisely determined Cabibbo-Kobayashi-Maskawa (CKM) factors. The result is then rescaled by the experimental value[6] of $B(b \to X\ell\nu) = 0.108$. The semi-leptonic rate is calculated incorporating both charm and non-charm modes, and includes both phase space and QCD corrections[7]. The calculation of $\Gamma(b \to s\gamma)$ employs the next-to-leading log evolution equations from Misiak[4] for the coefficients of the $b \to s$ transition operators in the effective Hamiltonian, gluon bremsstrahlung corrections[8], corrections[9] for $m_{top} > M_W$, a running α_{QED} evaluated at m_b, and the 3-loop evolution of the running α_s which is fitted to the global value[1] at the Z mass scale. The ratio of CKM elements in the scaled decay rate, $|V_{tb}V_{ts}/V_{cb}|$, is taken to be unity. The

*Work supported by the Department of Energy, Contract DE-AC03-76SF00515

Invited talk presented at the *XXIII International Symposium on Ultra-High Energy Multiparticle Phenomena*, Aspen, CO, September 12-17, 1993.

Wilson coefficients of the $b \to s$ operators are evaluated perturbatively at the W scale, where the matching conditions are imposed, and evolved down to the renormalization scale μ, usually taken to be m_b. The prediction for the $b \to s\gamma$ branching fraction as a function of the top-quark mass in the SM is shown in Fig. 1a, taking $\mu = m_b = 5\,\mathrm{GeV}$. The solid curve represents the corrected rate due to the next-to-leading log evolution of the operator coefficients, while the dashed curve corresponds to the leading log case. The next-to-leading order corrections decrease the QCD enhancements by $\sim 15\%$, which is exactly the behavior one would expect. Figure 1b displays the dependency of the branching fraction (for $m_t = 150\,\mathrm{GeV}$) on the choice of the renormalization scale for the Wilson coefficients. The uncertainty introduced by the choice of the value of m_b in calculating $B(b \to X\ell\nu)$ is also shown in this figure, where the dashed(solid, dash-dotted) curve corresponds to $m_b = 4.25(5.0, 5.25)\,\mathrm{GeV}$. Taking $m_b = 5\,\mathrm{GeV}$, we see that the $b \to s\gamma$ branching fraction increases by $\sim 15\%$ as the renormalization scale μ is varied from m_b to $m_b/2$. The overall variation in the SM prediction for $B(b \to s\gamma)$ due to the combined freedom of choice in μ and m_b can be as large as 40%! Clearly, when determining constraints on new physics from this decay, it is best to choose values for these parameters which yields the most conservative SM rate; here, we take $\mu = m_b = 5.0\,\mathrm{GeV}$.

The possibility of anomalous couplings between the top-quark and the gauge boson sector has been examined in the literature[10]. Future colliders such as the LHC and NLC can probe these effective couplings down to the level of $10^{-18} - 10^{-19}$ e-cm, but they rely on direct production of top-quark pairs, whereas $b \to s\gamma$ provides the opportunity to probe the properties of the top-quark before it is produced directly. If the t-quark has large anomalous couplings to on-shell photons and gluons, the resulting prediction[11] for the $b \to s\gamma$ rate would conflict with experiment. The most general form of the Lagrangian which describes the interaction between top-quarks and on-shell photons (assuming operators of dimension-five or less, only) is

$$\mathcal{L}_{t\bar{t}\gamma} = e\bar{t}\left[Q_t\gamma_\mu + \frac{1}{2m_t}\sigma_{\mu\nu}(\kappa_\gamma + i\tilde{\kappa}_\gamma\gamma_5)q^\nu\right]tA^\mu\,, \tag{1}$$

where Q_t is the electric charge of the t-quark, and $\kappa_\gamma(\tilde{\kappa}_\gamma)$ represents the anomalous magnetic (electric) dipole moment. A similar expression is obtained for $\mathcal{L}_{t\bar{t}g}$. Note that a non-vanishing value for $\tilde{\kappa}_\gamma$ would signal the presence of a CP-violating amplitude. In practice, only the coefficients of the magnetic dipole and chromo-magnetic dipole $b \to s$ transition operators, denoted as O_7 and O_8 respectively, are modified by the presence of these couplings. The coefficients of these operators at the W scale can be written as

$$\begin{aligned} c_7(M_W) &= G_7^{SM}(m_t^2/M_W^2) + \kappa_\gamma G_1(m_t^2/M_W^2) + i\tilde{\kappa}_\gamma G_2(m_t^2/M_W^2)\,, \\ c_8(M_W) &= G_8^{SM}(m_t^2/M_W^2) + \kappa_g G_1(m_t^2/M_W^2) + i\tilde{\kappa}_g G_2(m_t^2/M_W^2)\,. \end{aligned} \tag{2}$$

The functions G_i are obtained by inserting the above couplings into the Feymann diagrams in which the photon is emitted from the top-quark line, and extracting the pure dipole-like terms after performing the loop integrations and are given in [11]. All other Lorentz structures vanish due to electromagnetic gauge invariance and the fact that the photon is on-shell. When the resulting branching fraction and the CLEO data are combined, the constraints shown in Fig. 2 are obtained. In Fig. 2a, the 95% C.L. allowed region of the anomalous magnetic dipole operator as a function of m_t lies between the curves for the cases $\kappa_g = 0$ (solid curves) and $\kappa_g = \kappa_\gamma$ (dashed curves). In Fig. 2b, the 95% C.L. allowed region for the anomalous electric dipole moment lies beneath the curves. The bounds on the chromo-dipole moments are found to be weak, since they only enter the decay rate via operator mixing. For $m_t = 150\,\mathrm{GeV}$, κ_γ is constrained to lie in the range $(-2.6$ to $3.4) \times 10^{-16}$ e-cm, and $\tilde{\kappa}_\gamma < 5.1 \times 10^{-16}$ e-cm.

The trilinear gauge coupling of the photon to W^+W^- can also be tested by the $b \to s\gamma$ process. Anomalous γWW vertices can be probed by looking for deviations from the SM in tree-level processes such as $e^+e^- \to W^+W^-$ and $p\bar{p} \to W\gamma$, or by their influence on loop order processes, for example the $g-2$ of the muon. In the latter case, cutoffs must be used in order to regulate the divergent loop integrals and can introduce errors by attributing a physical significance to the cutoff[12].

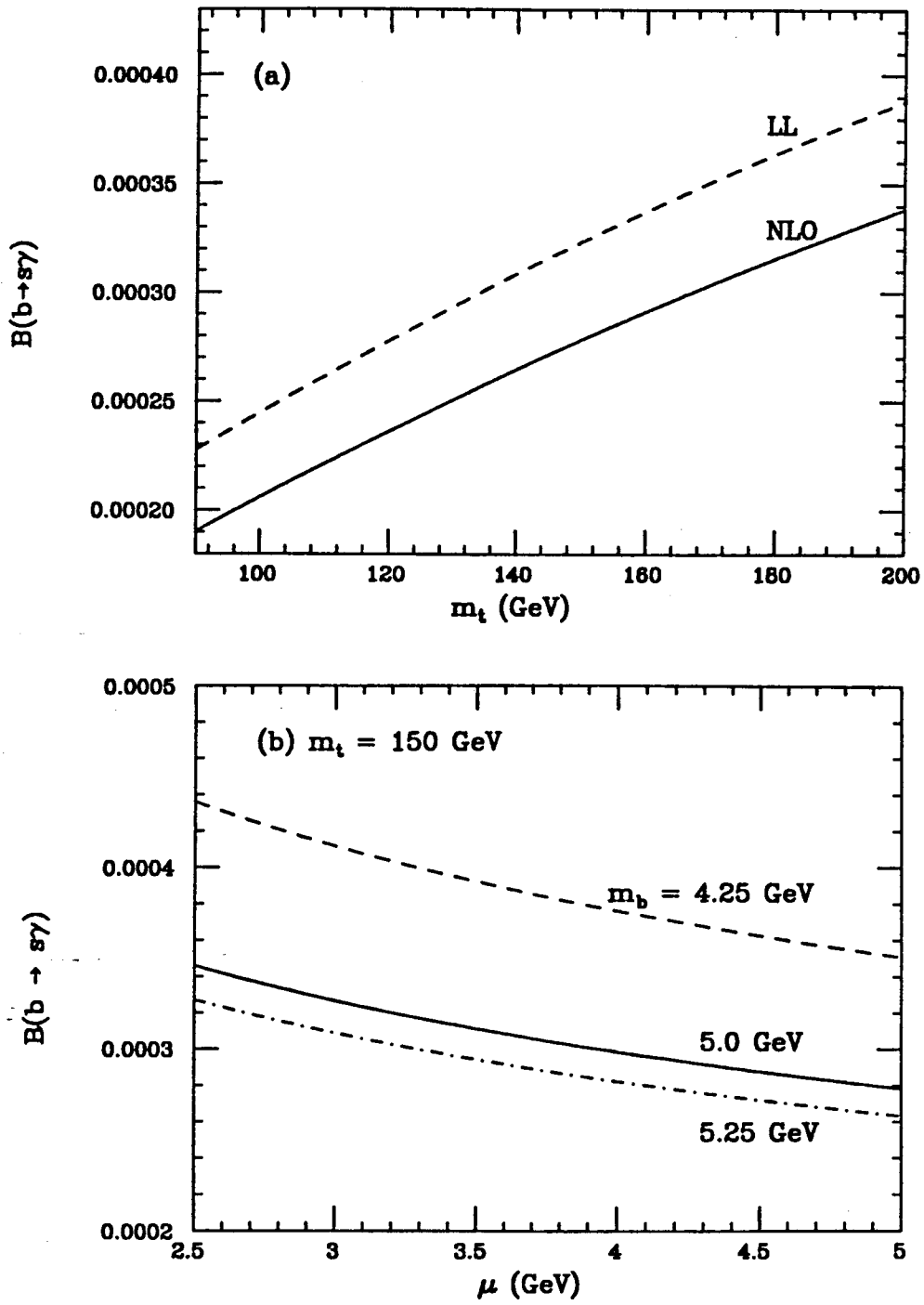

Fig. 1. The branching fraction for $b \to s\gamma$ in the Standard Model (a) as a function of the top-quark mass including QCD corrections to the leading log (dashed) and next-to-leading log order (solid). (b) Dependency of the branching fraction on the choice of renormalization scale μ for various values of the b-quark mass as indicated with $m_t = 150\,\mathrm{GeV}$.

However, some loop processes, such as $b \to s\gamma$, avoid this problem due to cancellations provided by the GIM mechanism, and hence yield cutoff independent bounds on anomalous couplings. The CP-conserving interaction Lagrangian for $WW\gamma$ interactions is

$$\mathcal{L}_{WW\gamma} = i\left(W^\dagger_{\mu\nu}W^\mu A^\nu - W^\dagger_\mu A_\nu W^{\mu\nu}\right) + i\kappa_\gamma W^\dagger_\mu W_\nu A^{\mu\nu} + i\frac{\lambda_\gamma}{M_W^2}W^\dagger_{\lambda\mu}W^\mu_\nu A^{\nu\lambda}\,, \tag{3}$$

where $V_{\mu\nu} = \partial_\mu V_\nu - \partial_\nu V_\mu$, and the two parameters $\kappa_\gamma = 1 + \Delta\kappa_\gamma$ and λ_γ take on the values $\Delta\kappa_\gamma, \lambda_\gamma = 0$ in the SM. In this case, only the coefficient of the magnetic dipole $b \to s$ transition operator, O_7, is modified by the presence of these additional terms and can be written as

$$c_7(M_W) = G_7^{SM}(m_t^2/M_W^2) + \Delta\kappa_\gamma A_1(m_t^2/M_W^2) + \lambda_\gamma A_2(m_t^2/M_W^2)\,. \tag{4}$$

The functions $A_{1,2}$ are obtained in the same manner as described above for the anomalous top-quark couplings and are given explicitly in Ref. [13]. As both of these parameters are varied, either large enhancements or suppressions over the SM prediction for the $b \to s\gamma$ branching fraction can be obtained. When one demands consistency with both the upper and lower CLEO bounds, a large region of the $\Delta\kappa_\gamma - \lambda_\gamma$ parameter plane is excluded; this is displayed in Fig. 3 from Rizzo[13] for $m_t = 150\,\text{GeV}$. Here, the 95% C.L. bounds obtained from the lower limit on $B(b \to s\gamma)$ correspond to the dashed curves, where the region between the curves is excluded, while the constraints placed from the upper CLEO limit correspond to the diagonal solid lines, with the allowed region lying in between the lines. The allowed region in this parameter plane as determined from UA2 data[14] from the reaction $pp \to W\gamma$ is also displayed in this figure and corresponds to the region between the two almost horizontal lines. Combining these constraints, an overall allowed region is obtained and is represented by the two shaded regions in this figure. We see that a sizable area of the parameter space is ruled out! Note that the SM point in the $\Delta\kappa_\gamma - \lambda_\gamma$ plane (labeled by 'S') lies in the center of one of the allowed regions.

Next we turn to two-Higgs-doublet models (2HDM), where we examine two distinct models which naturally avoid tree-level flavor changing neutral currents. In Model I, one doublet (ϕ_2) generates masses for all fermions and the other doublet (ϕ_1) decouples from the fermion sector. In the second model (Model II) ϕ_2 gives mass to the up-type quarks, while the down-type quarks and charged leptons receive their mass from ϕ_1. Each doublet obtains a vacuum expectation value (vev) v_i, subject to the constraint that $v_1^2 + v_2^2 = v^2$, where v is the usual vev present in the SM. The charged Higgs boson interactions with the quark sector are governed by the Lagrangian

$$\mathcal{L} = \frac{g}{2\sqrt{2}M_W}H^\pm\left[V_{ij}m_{u_i}A_u\bar{u}_i(1-\gamma_5)d_j + V_{ij}m_{d_j}A_d\bar{u}_i(1+\gamma_5)d_j\right] + H.c.\,, \tag{5}$$

where g is the usual SU(2) coupling constant and V_{ij} represents the appropriate CKM element. In model I, $A_u = \cot\beta$ and $A_d = -\cot\beta$, while in model II, $A_u = \cot\beta$ and $A_d = \tan\beta$, where $\tan\beta \equiv v_2/v_1$ is the ratio of vevs. In both models, $H^\pm$ contributes to $b \to s\gamma$ via virtual exchange together with the top-quark and the dipole $b \to s$ operators ($O_{7,8}$) receive contributions from this exchange. At the W scale the coefficients of these operators take the generic form

$$c_i(M_W) = G_i^{SM}(m_t^2/M_W^2) + \lambda A_{1_i}^{H^\pm}(m_t^2/m_{H^\pm}^2) + \frac{1}{\tan^2\beta}A_{2_i}^{H^\pm}(m_t^2/m_{H^\pm}^2)\,, \tag{6}$$

where $\lambda = -1/\tan\beta,\ +1$ in Model I and II, respectively, and $i = 7, 8$. The analytic form of the functions A_{1_i}, A_{2_i} can be found in [15]. Since the $H^\pm$ contributions all scale as $\cot^2\beta$ in Model I, enhancements to the SM decay rate only occurs for small values of $\tan\beta$. The relative minus sign between the two $H^\pm$ contributions in this model also gives a destructive interference for some values of the parameters. Consistency with the CLEO lower and upper limits excludes[16] the shaded regions in the $m_{H^\pm} - \tan\beta$ parameter plane presented in Fig. 4a, taking $m_t = 150\,\text{GeV}$. Here, the shaded region on the left results from the CLEO upper bound and the shaded slice in the middle

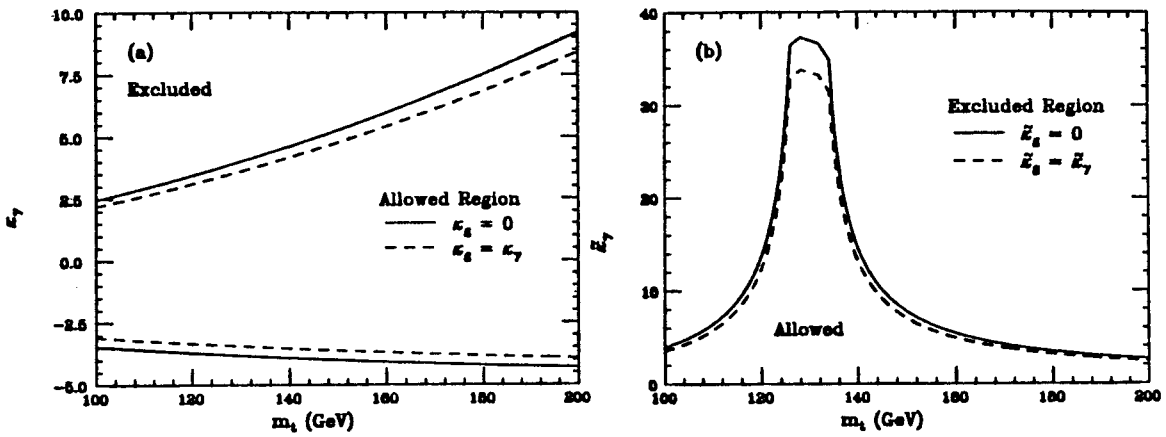

Fig. 2. The allowed range of (a) κ_γ and (b) $\tilde{\kappa}_\gamma$ assuming $\langle \tilde{\kappa}_g \rangle = 0$ (solid curve) or $\langle \tilde{\kappa}_g \rangle = \langle \tilde{\kappa}_\gamma \rangle$ (dashed curve).

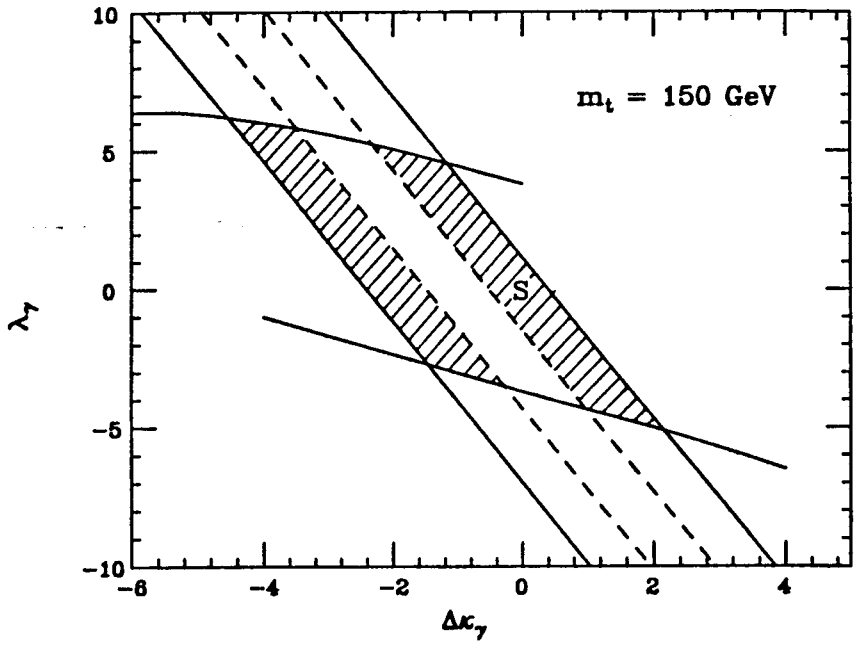

Fig. 3. Allowed (shaded) region of the $\Delta\kappa_\gamma - \lambda_\gamma$ parameter plane from the CLEO upper and lower bounds on $b \to s\gamma$, assuming $m_t = 150\,\mathrm{GeV}$, and the UA2 event rate for $pp \to W\gamma$ as discussed in the text. The point in this plane representing the SM is labeled by S.

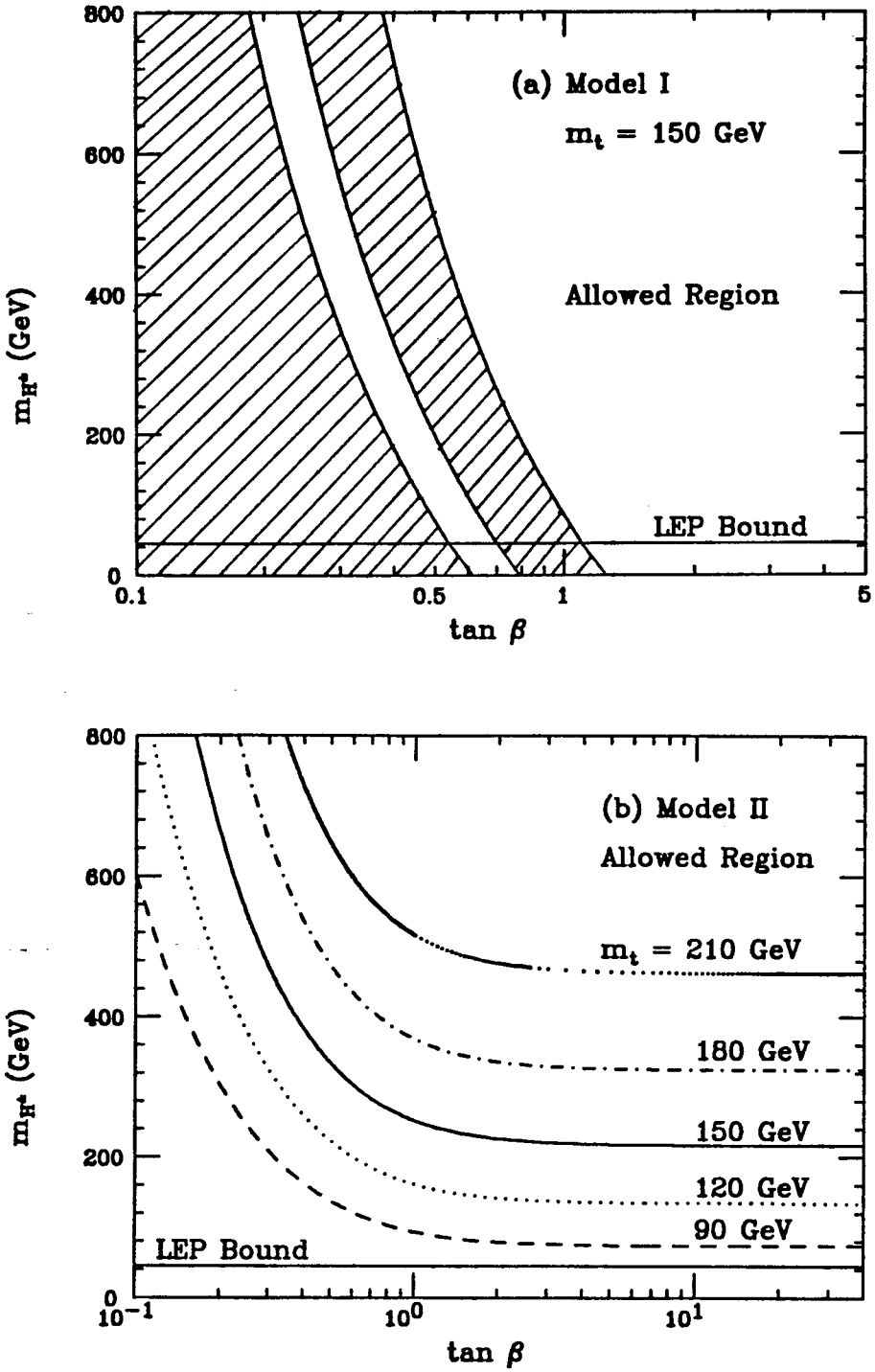

Fig. 4. The excluded regions in the $m_{H^\pm} - \tan\beta$ plane resulting from the present CLEO bounds in (a) Model I (shaded area is excluded) for $m_t = 150\,\text{GeV}$ and (b) Model II for various values of m_t as indicated, where the excluded regions lie to the left and below each curve.

is from the lower limit. In Model II, large enhancements also appear for small values of $\tan\beta$, but more importantly, $B(b \to s\gamma)$ is always larger than that of the SM, independent of the value of $\tan\beta$. This is due to the $+\tan\beta$ scaling of the $A_{1,}^{H^\pm}$ term in Eq. (6). In this case, the CLEO upper bound excludes[16, 17] the region to the left and beneath the curves shown in Fig. 4b, for various values of m_t as indicated. We note that the $H^\pm$ couplings present in Model II are of the type present in Supersymmetry. However, the limits obtained in supersymmetric theories also depend on the size of the other super-particle contributions to $b \to s\gamma$, and are generally much more complex[18].

In summary, we have seen that the process $b \to s\gamma$ provides powerful constraints for a variety of models containing physics beyond the SM. In most cases, these constraints either complement or are stronger than those from other low-energy processes and from direct collider searches.

References

1. See, for example, M. Swartz and W. Hollik, talks presented at the *XVI International Symposium on Lepton-Photon Interactions*, Cornell University, August 1993.
2. R. Ammar *et al.*, CLEO Collaboration, Phys. Rev. Lett, **71**, 674 (1993); E. Thorndike, CLEO Collaboration, talk presented at the *1993 Meeting of the American Physical Society*, Washington, D.C., April 1993.
3. C. Bernard, P. Hsieh, and A. Soni, Washington University Report Wash-U-HEP-93-35 (1993).
4. M. Misiak, Phys. Lett. **B269**, 161 (1991); Nucl. Phys. **B393**, 23 (1993); A.J. Buras, M. Misiak, M. Munz, and S. Pokorski, Max Planck Institute Report, MPI-PH-93-77.
5. For a collection of references on the effects of non-Standard Model physics on $b \to s\gamma$, see, for example, J.L. Hewett, talk presented at the *XXI SLAC Summer Institute*, July 26 - August 6, 1993, Stanford, CA.
6. P. Drell, plenary talk presented at the *XXVI International Conference on High Energy Physics*, Dallas, TX, August 1992.
7. N. Cabibbo and L. Maiani, Phys. Lett. **B79**, 109 (1978).
8. A. Ali and C. Greub, Phys. Lett. **B287**, 191 (1992).
9. P. Cho and B. Grinstein, Nucl. Phys. **B365**, 279 (1991).
10. D. Atwood, *et al.*, Phys. Rev. Lett. **69**, 2754 (1992); G. Kane, *et al.*, Phys. Rev. **D45**, 124 (1992); M. Peskin, talk presented at the *Second International Workshop on Physics and Experiments at Linear Colliders*, Waikoloa, HI, April 1993.
11. J.L. Hewett and T.G. Rizzo, Phys. Rev. **D49**, 319 (1994).
12. C.P. Burgess and D. London, Phys. Rev. Lett. **69**, 3428 (1992); McGill University Reports McGill-92/04 and -05 (1992).
13. T.G. Rizzo, Phys. Lett. **B315**, 471 (1993); S.-P. Chia, Phys. Lett. **B240**, 465 (1990); K.A. Peterson, Phys. Lett. **B282**, 207 (1992).
14. J. Alitti *et al.*, UA2 Collaboration, Phys. Lett. **B277**, 194 (1992).
15. B. Grinstein, R. Springer, and M. Wise, Nucl. Phys. **B339**, 269 (1990); T.G. Rizzo, Phys. Rev. **D38**, 820 (1988); W.-S. Hou and R.S. Willey, Phys. Lett. **B202**, 591 (1988); C.Q. Geng and J.N. Ng, Phys. Rev. **D38**, 2858 (1988); V. Barger, J.L. Hewett, and R.J.N. Phillips, Phys. Rev. **D41**, 3421 (1990).
16. J.L. Hewett, Phys. Rev. Lett. **70**, 1045 (1993).
17. V. Barger, M. Berger, and R.J.N. Phillips, Phys. Rev. Lett. **70**, 1368 (1993).
18. S. Bertolini, *et al.*, Nucl. Phys. **B294**, 321 (1987), and Nucl. Phys. **B353**, 591 (1991).